Journal of

Mechanics of Materials and Structures

THE SIMULATION OF RESIDUAL STRESSES IN FRICTION STIR WELDS

Zhao Zhang and Hongwu Zhang

Volume 2, Nº 5 *May 2007*

mathematical sciences publishers

JOURNAL OF MECHANICS OF MATERIALS AND STRUCTURES
Vol. 2, No. 5, 2007

THE SIMULATION OF RESIDUAL STRESSES IN FRICTION STIR WELDS

ZHAO ZHANG AND HONGWU ZHANG

A numerical model is developed to investigate energy dissipations and residual stress distributions in friction stir welds. Results indicate that the maximum longitudinal residual stress can be increased with the increase of the translational velocity of the pin. But the variation of the angular velocity of the pin does not significantly affect the residual stress distributions. Energy dissipation in friction is increased with the increase of the angular velocity of the pin. However, with the increase of the translational velocity of the pin the plastic dissipation of energy is increased and the frictional dissipation is decreased.

1. Introduction

Friction stir welding (FSW) is a new solid-state joining technology invented by the Welding Institute (TWI) in 1991 [Thomas et al. 1991]. Compared with conventional welding processes, FSW has many advantages such as no melting, low defects, and low distortion, and can even join thin and thick sections. This new technique has been successfully applied to the aerospace, automobile, and shipbuilding industries.

Temperatures near the rotating pin never reach the melting point in FSW [Tang et al. 1998], and quite complicated flow was observed in welds [Murr et al. 1998; Xu et al. 2001]. Colligan [1999] studied the material flow in 6061 and 7075 aluminum by imbedding small steel balls as tracers into grooves cut into the work piece parallel to the weld line. Murr et al. [1999] and Li et al. [1999] found that dynamic recrystallization plays a key role in material movement. The joining of Al 6061 alloy to AISI 1018 steel by the combined effect of fusion and solid state welding was investigated by Chen and Kovacevic [2004]. It was found that the intermetallic phases $Al_{13}Fe_4$ and Al_5Fe_2 exist in the weld zone.

The temperature field in friction stir welding was studied by Song and Kovacevic [2003] and Chen and Kovacevic [2003] using a finite element method. It was shown that the preheating into the work piece is beneficial to FSW. Dalle Donne et al. [2000] found that the residual stress of the weld affects the fatigue properties. Webster et al. [2001] reported the measurement of residual stress in FSW by the X-ray technique and found that the longitudinal residual stress varies in the range from 60 to 140 MPa. Sutton et al. [2002] investigated the residual stress in 2024-T3 aluminum friction stir butt welds using the neutron diffraction technique. The results show that the highest stress occurs near the crown side of the weld over the entire FSW region. Peel et al. [2003] further gave the results of microstructure, mechanical property and residual stress of four aluminum AA5083 friction stir welds produced under varying conditions.

Keywords: friction stir welding, residual stress, finite element method, energy dissipation.
This work is supported by the National Natural Science Foundation of China (nos. 10302007, 10421202, and 10225212), the Program for Changjiang Scholars and the Innovative Research Team in the University of China (PCSIRT) and the National Key Basic Research Special Foundation of China (no. 2005CB321704).

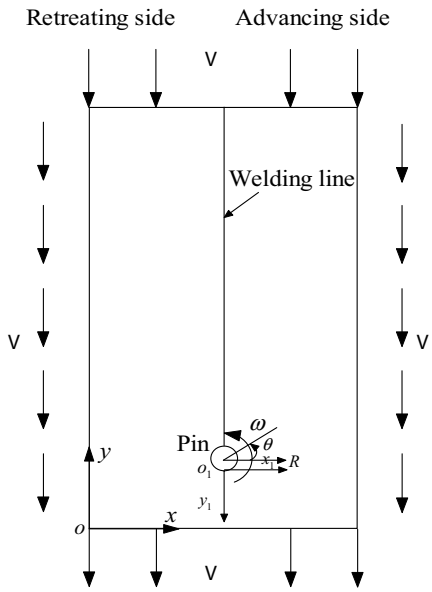

Figure 1. The geometry model and boundary conditions of FSW.

Zhu and Chao [2004] reported the transient temperature and residual stresses of 304L stainless steel. The distribution and the influence of residual stresses on fatigue in FSW were investigated by James et al. [2004]. Reynolds et al. [2003] reported the residual stress distribution of 304L steel under different angular velocities. A two dimensional modeling of FSW, based on the Arbitrary Lagrangian–Eulerian (ALE) finite element formulation, was reported by Deng and Xu [2001]. The method was further extended to analyze the three dimensional material flow by Xu and Deng [2002]. In the numerical models established by Deng and Xu, rate-independent material was used to model the friction stir welding process. It was found that the rate-independent material is appropriate enough to model the material behaviors in FSW process.

So far, there are no successful in-depth numerical reports on residual stress distributions in friction stir welds in different process parameters, including welding speed and angular velocity. A new numerical method, that is, transferring the results from a dynamic solver into a static one to obtain the residual stress on the friction stir weld after the FSW process, is herein proposed to investigate the residual stress distributions in the present research. Two approaches are needed to reduce the computational costs: one is to use the experimental data of the temperature field in the friction stir welds; the other is to increase the boundary conditions by 1000 times. Comparison with experimental tests on residual stresses in friction stir welds in the existing literature can validate the numerical model developed.

2. Model description

In FSW the material of the work piece in front of the tool is pushed aside by the pin and is forced to flow by the action of the pin, around which large plastic flow develops. In order to model the contacting surface properly and handle mesh distortion during large plastic deformation, a thermo-mechanical

finite element method, based on the Arbitrary Lagrangian–Eulerian (ALE) formulation and the adaptive remeshing technique, is employed. By means of ALE, material surfaces can be tracked with the accuracy characteristic of the Lagrangian methods and the interior mesh can be fixed in some directions so as to avoid element distortion and entanglement. The mesh should be prescribed so that the boundaries and interfaces remain at least partially Lagrangian.

The radius of the pin R_0 is 3 mm, and the dimensions of the two plates are 100 mm in length (along the welding line) and 30 mm in width (see Figure 1). Such a small welding plate has been proven to precisely predict the material behaviors [Deng and Xu 2004; Zhang et al. 2005b] by tracing the material particles near the rotating tool and the tool forces applied on the shoulder [Ulysse 2002]. The main advantage of such a small welded plate is that the computational cost can be greatly reduced. The same size welded plate is used in the present research for the investigation on material velocity field near the rotating pin and the residual stress distribution on the friction stir weld. The two dimensional geometry is discretized into four-node quadrilateral elements. Reduced integration with hourglass control is used to avoid the mesh-locking problems associated with large incompressible plastic deformation. The mesh consists of 11717 elements and 11986 nodes. The material of the plate is AL 6061-T6, as a rate independent elasto-plastic material. However, the effect of temperature on yielding is considered explicitly. The properties of the material at different temperatures are shown in Table 1 [Brown et al. 1993].

The constitutive relations are given by the von Mises yield criterion and the associated flow rule. The von Mises yield condition can be expressed as

$$F_d(\sigma_{ij}, \bar{\varepsilon}) = \frac{1}{2}\sigma'_{ij}\sigma'_{ij} - \frac{1}{3}\sigma_s^2(\bar{\varepsilon}), \tag{1}$$

where $\boldsymbol{\sigma}'$ is the deviatoric part of Kirchhoff stress. $\bar{\varepsilon}$ represents the equivalent plastic strain and σ_s is the yield stress of the material.

For an associate flow, the direction of the plastic flow $\boldsymbol{n}_s$ is normal to the flow potential F_d as

$$\boldsymbol{n}_s = \frac{\partial \boldsymbol{F}_d/\partial\boldsymbol{\sigma}}{\|\partial \boldsymbol{F}_d/\partial\boldsymbol{\sigma}\|} = \frac{\boldsymbol{D}_p}{\|\boldsymbol{D}_p\|}, \tag{2}$$

where $\boldsymbol{D}_p$ represents the inelastic rate of deformation, and $\|\boldsymbol{D}_p\| = (\boldsymbol{D}_p : \boldsymbol{D}_p)^{1/2}$.

T (°C)	E (GPa)	σ_u (MPa)	ν
25.00	66.94	278.12	0.330
100.00	63.21	260.68	0.334
148.89	61.32	251.24	0.335
204.44	56.80	221.01	0.336
260.00	51.15	152.26	0.338
315.56	47.17	73.87	0.360
371.11	43.51	36.84	0.400
426.67	28.77	21.58	0.410
482.22	20.20	10.49	0.420

Table 1. Temperature-dependent material properties of AL6061-T6.

The flow rule has the form

$$\boldsymbol{D}^p = \dot{\lambda}\frac{3\boldsymbol{\sigma}'}{2\bar{\sigma}}, \tag{3}$$

where $\dot{\lambda}$ denotes the scalar measuring of the rate of inelastic flow, and $\bar{\sigma}$ denotes the equivalent stress, $\bar{\sigma} = [\frac{3}{2}\boldsymbol{\sigma}' : \boldsymbol{\sigma}']^{1/2}$.

The Jaumann rate of the Kirchhoff stress tensor is given as

$$\boldsymbol{\sigma}^{\nabla J} = \dot{\boldsymbol{\sigma}} - \boldsymbol{W}\cdot\boldsymbol{\sigma} + \boldsymbol{\sigma}\cdot\boldsymbol{W}, \tag{4}$$

where the additive decomposition of the rate of deformation tensor $\boldsymbol{D}$ into elastic and plastic components is implied, that is, $\boldsymbol{D} = \boldsymbol{D}^e + \boldsymbol{D}^p$. $\boldsymbol{W}$ is the rate of spin tensor. The rate of deformation is defined as the symmetric part of the velocity gradient, $\boldsymbol{D} = \frac{1}{2}((\nabla\boldsymbol{v})^T + \nabla\boldsymbol{v})$, and the rate of spin tensor is the skew symmetric part, $\boldsymbol{W} = \frac{1}{2}((\nabla\boldsymbol{v})^T - \nabla\boldsymbol{v})$.

2.1. ***Definition of contact.*** The frictional contact model is used. The interface may experience frictional contact described by a modified Coulomb friction law. The Coulomb friction law is modified so that there exists a maximum critical frictional stress, above which the frictional stress stays constant and is no longer equal to the product of the friction coefficient and the contact pressure. A reasonable upper bound $\tau_{\max} = \sigma_s/\sqrt{3}$ is used.

2.2. ***Boundary conditions.*** At the boundaries of the plates, material particles move with a constant speed $\boldsymbol{v}$ relative to the pin, as shown in Figure 1. The pin rotates with an angular velocity ω. It has been proved that the FSW process is in a steady state [Deng and Xu 2004; Zhang et al. 2005b]. So FSW can be treated as a quasistatic problem and the loading speed can be increased to save computational costs. In the present research, both the translational velocity and the angular velocity are increased 1000 times to accelerate convergence. In my previous work, the material flow patterns during the friction stir welding process have been investigated in detail [Zhang et al. 2005a; 2005b; Zhang and Zhang 2005] and the results can correlate well with the experimental tests [Guerra et al. 2002]. The computational results obtained in my previous work [Zhang et al. 2005b] are transferred from ABAQUS/Explicit to ABAQUS/Standard in the present research. The obtained results from the dynamic solver are transferred to the static solver and then are treated as a static problem to obtain the residual stress distributions in the friction stir weld. In this process, the fixtures are released and the temperature is reduced to room temperature.

2.3. ***Integration method.*** The simplest operator that provides unconditional stability for integration equations is the backward Euler method. The strain rate decomposition is integrated over a time increment as

$$\Delta\varepsilon = \Delta\varepsilon^{el} + \Delta\varepsilon^{pl}, \tag{5}$$

where $\Delta\varepsilon$ is defined by central difference operator

$$\Delta\varepsilon = \operatorname{sym}\left[\frac{\partial\Delta x}{\partial\left(x_t + \frac{1}{2}\Delta x\right)}\right].$$

During the solution, the elasticity relationship and the integrated rate decomposition are satisfied exactly, so that

$$c_\sigma = -D^{el} : c_\varepsilon, \tag{6}$$

where c_σ is the correction to the stress, c_ε is the correction to the plastic strain increments, and $D^{el} = \frac{\partial^2 U}{\partial \varepsilon^{el} \partial \varepsilon^{el}}$ is the tangent elasticity matrix.

If hardening laws are considered, then

$$c_\alpha = h_\alpha c_\lambda + \Delta\lambda \left(\frac{\partial h_\alpha}{\partial \sigma} : c_\sigma + \frac{\partial h_\alpha}{\partial H_\beta} c_\beta \right), \tag{7}$$

where c_α is the correction to ΔH_α, and c_λ is the correction to $\Delta\lambda$.

The flow rule is not satisfied exactly until the following solution has been found

$$c_\varepsilon - c_\lambda \frac{\partial g}{\partial \boldsymbol{\sigma}} - \Delta\lambda \left(\frac{\partial^2 g}{\partial \boldsymbol{\sigma} \partial \boldsymbol{\sigma}} : c_\sigma + \frac{\partial^2 g}{\partial \boldsymbol{\sigma} \partial H_\alpha} c_\alpha \right) = \Delta\lambda \frac{\partial g}{\partial \boldsymbol{\sigma}} - \Delta \boldsymbol{\varepsilon}^{pl}. \tag{8}$$

The Newton–Raphson iteration method is applied until the flow equation and yield constraints are satisfied.

2.4. ***Temperature field.*** The heat generated at the interface between the shoulder and the work piece in FSW is the driving force to make FSW successful [Chao et al. 2003]. The heat flux must keep the maximum temperature in the work piece high enough so that the material is sufficiently soft to be stirred but low enough so that the material does not melt. The maximum temperature created by FSW ranges from 80% to 90% of the melting temperature of the welding material, as measured by Tang et al. [1998] and Colegrove et al. [2000].

The limitation of the PC computing power makes a fully thermo-mechanical analysis difficult to be completed in a reasonably short time [Deng and Xu 2001; Xu and Deng 2002]. To compensate for the lack of a predicted temperature field, actual temperature values from the practical FSW test [McClure et al. 1999] will be used to construct an approximate temperature field for the FSW process simulation, as shown in Figure 2. A tool rotation of 400rpm and a translational velocity of 2 mm/s are used in this experiment. Due to the limitation of the melting point of the material, the temperature fields near the pin under different cases do not have significant differences. So the same temperature field is used to model the friction stir welding process under different cases in the present analysis.

To show the reasonableness of the predicted temperature field, Figure 3 shows the predicted temperature field when the rotational velocity is 400 rpm before the translational movement of the pin. The maximum temperature occurs on the pin-plate interface. This is a quasistatic temperature field and the temperature distribution in the longitudinal direction perpendicular to the welding line scarcely varies with time. When the approximate temperature field is constructed, the pin starts to move along the welding line.

3. Results and discussion

Figure 4 shows the distribution of the residual stresses in the direction perpendicular to the welding line at $y_1 = 1$ mm, $y_1 = 2$ mm, and $y_1 = 3$ mm when $v = 2$ mm/s and $\omega = 390$ RPM. The maximum of the longitudinal residual stress occurs near $(R_0 + 1)$ mm away from the welding line. The longitudinal residual stress ranges from -100 MPa to about 100Mpa. The results can be validated in [Dalle Donne et al. 2001; Hornbach et al. 2003; Staron et al. 2004]. It seems that the maximum longitudinal residual stress occurs in the location where the equivalent plastic strain is decreased suddenly, as shown in Figure

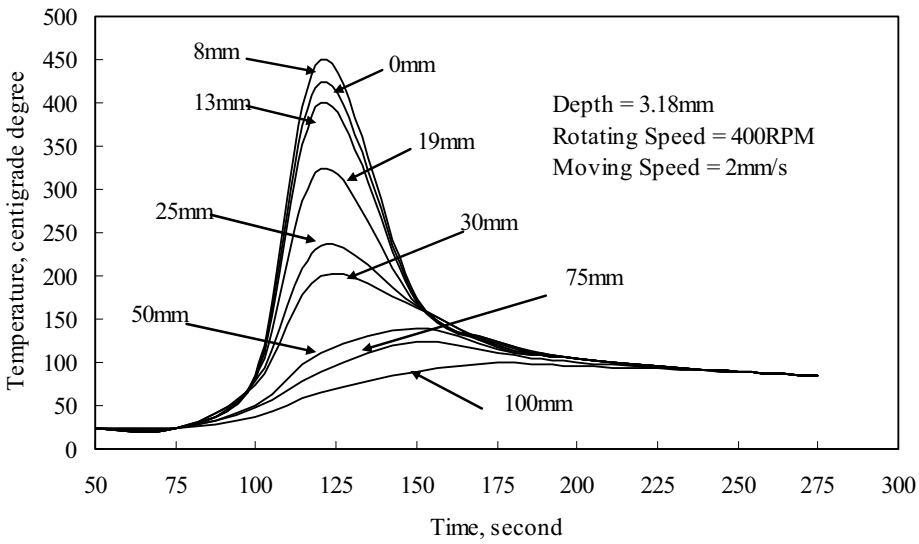

Figure 2. Fitted temperature history at various distances from the weld line.

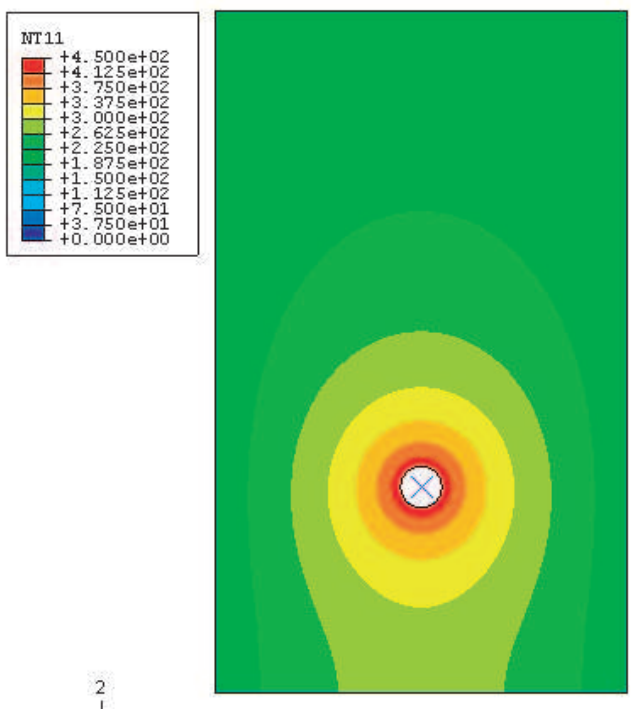

Figure 3. Predicted temperature field according to the experimental data.

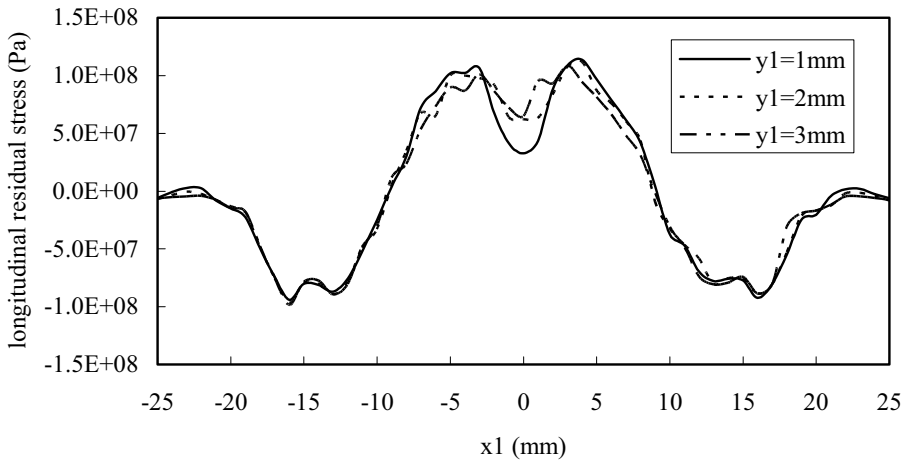

Figure 4. The distributions of the longitudinal residual stress in the direction perpendicular to the welding line ($v = 2$ mm/s, $\omega = 390$ RPM).

5. The region of large tensile residual stress can correlate well with that of large equivalent plastic strain. It is found that in the region where the equivalent plastic strain is decreasing, longitudinal residual stress is also decreasing. When away from the exaction point of the pin, the longitudinal residual stress in the welding line is slightly increasing. But after about 2 mm, distribution of the longitudinal residual stress remains steady. This means that the distributions of the longitudinal residual stress are not affected by the exaction of the pin after 2 mm away from the extraction point. The ratio of the maximum longitudinal residual stress to the initial yield stress is only about 39%, which is much lower than the one obtained in the welds produced by the traditional welding techniques. The residual stresses are not symmetric to the welding line because the deformations are clearly unsymmetric. When the fixtures are released and the temperature is reduced to room temperature, the material in the nugget zone tends to recover. But the material in the heat affected zone has smaller deformation and will prevent the recovery process in the nugget zone. So the maxima of longitudinal residual stress occur in the boundaries of the heat affected zone with a minimum in the nugget zone. The deformations on the retreating side and the advancing side differ, causing the recovery processes to differ too. So the residual stress cannot be symmetric to the welding line.

Figure 6 shows the distributions of the longitudinal residual stress under different translational velocities in the direction perpendicular to the welding line. It is clear that the longitudinal residual stress is increased with the increase of the translational velocity in the tensile region, which can correlate well with the observations from experiments [Peel et al. 2003]. But at points where $x_1 = \pm 16$ mm, the longitudinal residual stress is not affected by the increase of the translational velocity. In the compressive region, it is difficult to judge the effect of the increase of the translational velocity. But in fact, the region of the large tensile stress is much more interesting since it is much closer to the welding line. Compared with the results in Figure 4, the maximum of the longitudinal residual stress occurs only near $(R_0 + 1)$ mm, which is about 140 MPa. The ratio of the maximum longitudinal residual stress to the initial yield stress

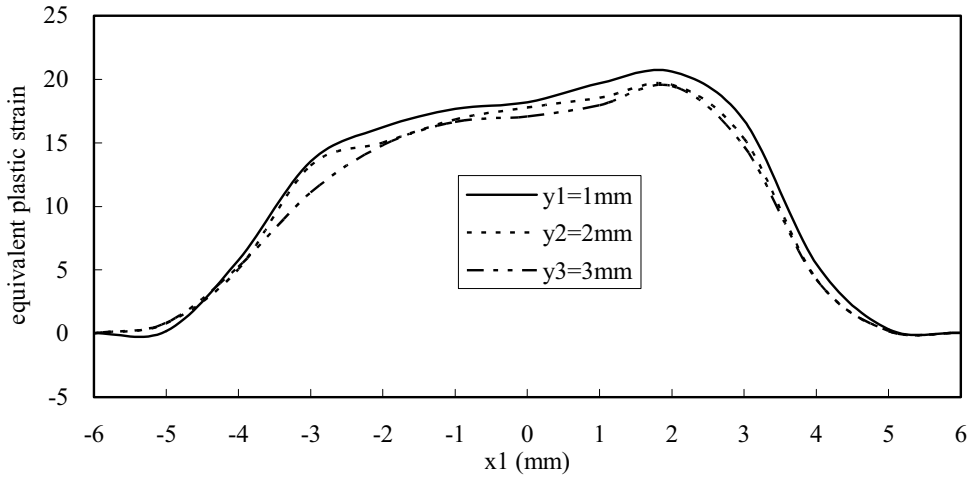

Figure 5. The distributions of the equivalent plastic strain in the direction perpendicular to the welding line ($v = 2$ mm/s, $\omega = 390$ RPM).

is also increased approximately from 41% to 50% when the translational velocity of the pin is increased from 4 mm/s to 10 mm/s.

Figure 7 shows the distributions of the longitudinal residual stress under different angular velocities in the direction perpendicular to the welding line. With the increase of the angular velocity, the large tensile region is moved to the advancing side. By experiments, Dalle Donne et al. [2001] found that the maximum longitudinal residual stress occurs on the advancing side. Both the numerical modeling in the present research and Dalle Donne's experiment lead to the same conclusion, that is, that the maximum longitudinal residual stress can occur at the advancing side instead of the retreating side, which can

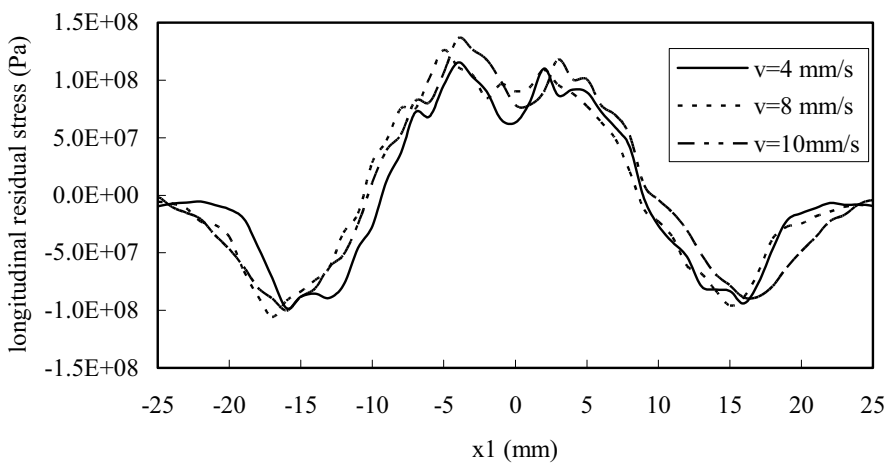

Figure 6. The distributions of the longitudinal residual stress under different translational velocities in the direction perpendicular to the welding line ($\omega = 390$ RPM).

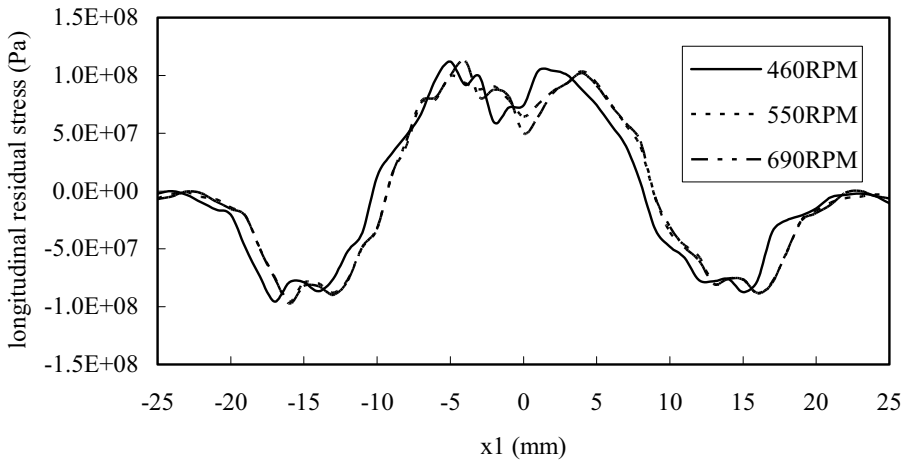

Figure 7. The distributions of the longitudinal residual stress under different angular velocities in the direction perpendicular to the welding line ($v = 2$ mm/s).

validate the numerical model established. There is a concave point near the welding line. The change of the angular velocity can affect the location of the concave point. With the increase of the angular velocity, the concave point can be moved to the advancing side. In summary, the effect of the change of the angular velocity on the longitudinal residual stress is not clear, which can be fitted well with experiments on residual stress in friction stir welding [Reynolds et al. 2003]. So, the variation of the angular velocity does not significantly affect the ratio of maximum longitudinal residual stress to the initial yield stress.

When the translational velocity of the pin is smaller, the maximum longitudinal residual stress on the retreating side and the one on the advancing side are similar, as shown in Figure 4. But with the increase of the translational velocity of the pin, the maximum longitudinal residual stress on the retreating side becomes higher than that on the advancing side. The maximum longitudinal residual stress can be increased from 100 MPa to about 140 MPa when the translational velocity is increased to 10 mm/s.

Remark. The residual stress distributions of friction stir welds have been studied by experiments reported in [Dalle Donne et al. 2001; Hornbach et al. 2003; Reynolds et al. 2003; Staron et al. 2004]. It was found that the curve of the longitudinal residual stress has a feature of a double peak. The maxima of the residual stress occur in the boundaries of the heat affected zone. The distributions of the longitudinal residual stress obtained from the present numerical model can correlate well with those in the experiments. The longitudinal residual stresses of 6XXX alloys range from -60 MPa to $+100$ MPa [Dalle Donne et al. 2001], which are very similar to those obtained in the present research, as shown in Figure 8. The residual stresses can differ due to the different measurement method. It should be noted that this is a weak comparison due to the differences between experimental and numerical conditions. In particular, the shoulder effect is not considered in the present research. To reveal the residual stress distributions correctly, a three-dimensional model of FSW is needed for further investigation of residual stresses.

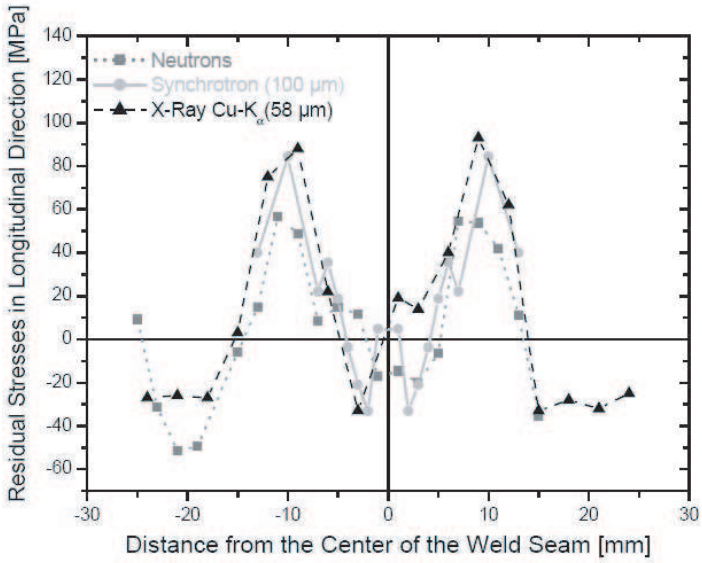

Figure 8. Longitudinal residual stresses measured by different published methods [Dalle Donne et al. 2001].

For better understanding of the mechanism of FSW, it is necessary to study the energy dissipations in FSW under different cases. It is known that the major energy dissipations in FSW are frictional ones and plastic ones. The energy dissipations under different process parameters are shown in Figure 9. It can be seen that the frictional dissipation of energy increases with the increase of the angular velocity of the pin. A possible explanation is that more revolutions are performed for the same length of the weld seam when the angular velocity of the pin is increased. For instance, the frictional dissipation is about 7×10^4 J at $t = 3.1 \times 10^{-3}$ s when $\omega = 460$ RPM, while the dissipation at the same t is 8.5×10^4 J when $\omega = 550$ RPM. The dissipation can be increased to 10.5×10^4 J at $t = 3.1 \times 10^{-3}$ s when $\omega = 690$ RPM. But the increase of the angular velocity of the pin does not affect the plastic dissipation which remains the same in Figures 9a–c.

The increase of the translational velocity of the pin does have an apparent effect on the plastic dissipation in FSW. The plastic dissipation can be increased with the increase of the translational velocity of the pin, but at the same time the frictional dissipation of energy is decreased, as shown in Figures 9d–f. The possible explanation is that with the increase of the translational velocity, the material deformation becomes more severe in the same time interval. So the plastic deformation of the material in the weld plates absorbs more energy. For instance, the frictional dissipation is 1.4×10^4 J and the plastic dissipation is 0.8×10^4 J at $t = 0.8 \times 10^{-3}$ s when $v = 4$ mm/s. When $v = 8$ mm/s, the frictional dissipation is 1.02×10^4 J and the plastic dissipation is 1.2×10^4 J at $t = 0.8 \times 10^{-3}$ s. When $v = 10$ mm/s, the frictional dissipation is 0.98×10^4 J and the plastic dissipation is 1.3×10^4 J at $t = 0.8 \times 10^{-3}$ s.

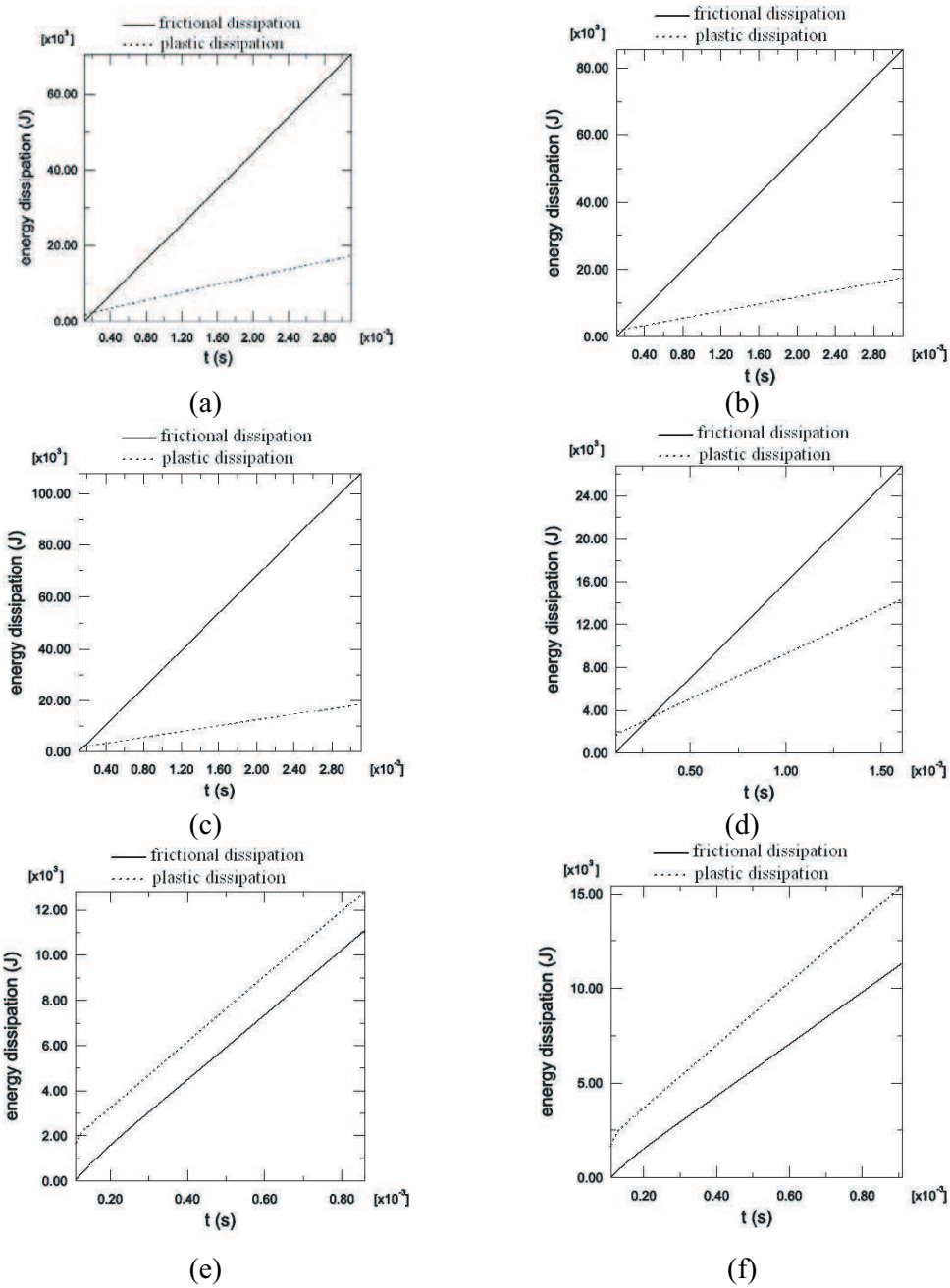

Figure 9. The energy dissipations in FSW under different cases: (a) $v = 2$ mm/s, $\omega = 460$ RPM, (b) $v = 2$ mm/s, $\omega = 550$ RPM, (c) $v = 2$ mm/s, $\omega = 690$ RPM, (d) $v = 4$ mm/s, $\omega = 390$ RPM, (e) $v = 8$ mm/s, $\omega = 390$ RPM, (f) $v = 10$ mm/s, $\omega = 390$ RPM.

4. Conclusions

The finite element method can be successfully applied to the modeling of residual stress distributions in friction stir welds. The results obtained in this paper are as follows:

(1) The maximum of the longitudinal residual stress occurs in the location where the equivalent plastic strain is decreased.

(2) The maximum longitudinal residual stress can be increased with the increase of the translational velocity of the pin, but the rotational velocities do not significantly affect the magnitude of the longitudinal residual stresses.

(3) The energy dissipation on friction is increased with the increase of the angular velocity of the pin. However, with the increase of the translational velocity of the pin the plastic dissipation is increased and the frictional dissipation is decreased.

Acknowledgments

The authors would like to thank Prof. X. M. Deng and Dr. S. W. Xu at the University of South Carolina for their helpful suggestions regarding the present research.

References

[Brown et al. 1993] W. F. Brown, H. Jr. Mindlin, and C. Y. Ho, *Aerospace structural metals handbook*, CINDAS/Purdue University, 1993.

[Chao et al. 2003] Y. J. Chao, X. Qi, and W. Tang, "Heat transfer in friction stir welding – experimental and numerical studies", *J. Manuf. Sci. Eng. (Trans. ASME)* **125**:1 (2003), 138–145.

[Chen and Kovacevic 2003] C. M. Chen and R. Kovacevic, "Finite element modeling of friction stir welding – thermal and thermomechanical analysis", *Int. J. Mach. Tools Manuf.* **43**:13 (2003), 1319–1326.

[Chen and Kovacevic 2004] C. M. Chen and R. Kovacevic, "Joining of Al 6061 alloy to AISI 1018 steel by combined effects of fusion and solid state welding", *Int. J. Mach. Tools Manuf.* **44**:11 (2004), 1205–1214.

[Colegrove et al. 2000] P. Colegrove, M. Painter, D. Graham, and T. Miller, "3 dimensional flow and thermal modeling of the friction stir welding process", in *Second international symposium on friction stir welding* (Gothenburg, Sweden), TWI, Cambridge, 2000.

[Colligan 1999] K. Colligan, "Material flow behavior during friction stir welding of aluminum", *Weld. J.* (July 1999), 229–237 (supplement, *Welding Research*).

[Dalle Donne et al. 2000] C. Dalle Donne, G. Biallas, T. Ghidini, and G. Raimbeaux, "Effect of weld imperfections and residual stresses on the fatigue crack propagation in friction stir welded joints", in *Second international symposium on friction stir welding* (Gothenburg, Sweden), TWI, Cambridge, 2000.

[Dalle Donne et al. 2001] C. Dalle Donne, E. Lima, J. Wegener, A. Pyzalla, and T. Buslaps, "Investigation of residual stresses in friction stir welds", in *Third international symposium on friction stir welding* (Kobe, Japan), TWI, Cambridge, 2001.

[Deng and Xu 2001] X. Deng and S. Xu, "Solid mechanics simulation of friction stir welding process", *Trans. NAMRI/SME, SME* **XXIX** (2001), 631–638.

[Deng and Xu 2004] X. M. Deng and S. W. Xu, "Two-dimensional finite element simulation of material flow in the friction stir welding process", *J. Manuf. Process.* **6**:2 (2004), 125–133.

[Guerra et al. 2002] M. Guerra, C. Schmidt, J. C. McClure, L. E. Murr, and A. C. Nunes, "Flow patterns during friction stir welding", *Mater. Charact.* **49**:2 (2002), 95–101.

[Hornbach et al. 2003] D. Hornbach, M. Mahoney, P. Prevey, D. Waldron, and J. Cammett, "Low plasticity burnishing of friction stir welds in 2219 aluminum to increase corrosion fatigue life", pp. 302–306 in *Trends in welding research, proceedings of the 6th international conference* (Phoenix, 2002), edited by S. A. David et al., ASM International, Materials Park, OH, 2003.

[James et al. 2004] M. N. James, D. G. Hattingh, D. J. Hughes, L. W. Wei, E. A. Patterson, and J. Quinta Da Fonseca, "Synchrotron diffraction investigation of the distribution and influence of residual stresses in fatigue", *Fatigue Fract. Eng. Mater. Struct.* **27**:7 (2004), 609–622.

[Li et al. 1999] Y. Li, L. E. Murr, and J. C. McClure, "Flow visualization and residual microstructures associated with the friction stir welding of 2024 and 6061 aluminum", *Mater. Sci. Eng. A* **271**:1-2 (1999), 213–223.

[McClure et al. 1999] J. C. McClure, Z. Feng, W. Tang, J. E. Gould, L. E. Murr, and X. Guo, "A thermal model of friction stir welding", pp. 590–596 in *Trends in welding research, proceedings of the 5th international conference* (Pine Mountain, GA, 1998), edited by J. M. Vitek et al., ASM International, Materials Park, OH, 1999.

[Murr et al. 1998] L. E. Murr, Y. Li, and R. D. Flores, "Intercalation vortices and related microstructural features in the friction stir welding of dissimilar metals", *Mater. Res. Innov.* **2**:3 (1998), 150–163.

[Murr et al. 1999] L. E. Murr, E. A. Trillo, Y. Li, R. D. Flores, B. M. Nowak, and J. C. McClure, "Solid-state flow associated with the friction stir welding of dissimilar metals", pp. 31–36 in *Fluid flow phenomena in metals processing* (San Diego, 1999), edited by N. El-Kaddah et al., Warrendale, PA, 1999.

[Peel et al. 2003] M. Peel, A. Steuwer, M. Preuss, and P. J. Withers, "Microstructure, mechanical properties and residual stresses as a function of welding speed in aluminium AA5083 friction stir welds", *Acta Mater.* **51**:16 (2003), 4791–4801.

[Reynolds et al. 2003] A. P. Reynolds, W. Tang, T. Gnaupel-Herold, and P. H., "Structure, properties and residual stress of 304L stainless steel friction stir welds", *Scr. Mater.* **48**:9 (2003), 1289–1294.

[Song and Kovacevic 2003] M. Song and R. Kovacevic, "Thermal modeling of friction stir welding in a moving coordinate system and its validation", *Int. J. Mach. Tools Manuf.* **43**:6 (2003), 605–615.

[Staron et al. 2004] P. Staron, M. Kocak, S. Williams, and A. Wescott, "Residual stress in friction stir-welded Al sheets", *Physica B Condens. Matter* **350**:1-3 (2004), e491–e493.

[Sutton et al. 2002] M. A. Sutton, A. P. Reynolds, D. Q. Wang, and C. R. Hubbard, "A study of residual stresses and microstructure in 2024-T3 aluminum friction stir butt welds", *J. Eng. Mater. Technol. (Trans. ASME)* **124**:2 (2002), 215–221.

[Tang et al. 1998] W. Tang, X. Guo, J. C. McClure, and L. E. Numes, "Heat input and temperature distribution in friction stir welding", *J. Mater. Process. Manuf. Sci.* **7**:2 (1998), 163–172.

[Thomas et al. 1991] W. M. Thomas, E. D. Nicholas, J. C. Needham, M. G. Murch, P. Templesmith, and C. J. Dawes, "Friction stir welding", International Patent Application No. PCT/GB92102203 and Great Britain Patent Application No. 9125978.8, 1991.

[Ulysse 2002] P. Ulysse, "Three-dimensional modeling of the friction stir welding process", *Int. J. Mach. Tools Manuf.* **42**:14 (2002), 1549–1557.

[Webster et al. 2001] P. J. Webster, L. Djapic Oosterkamp, P. A. Browne, D. J. Hughes, W. P. Kang, P. J. Withers, and G. B. M. Vaughan, "Synchrotron X-ray residual strain scanning of a friction stir weld", *J. Strain Anal. Eng. Des.* **36**:1 (2001), 61–70.

[Xu and Deng 2002] S. Xu and X. Deng, "A three-dimensional model for the friction stir welding process", pp. 699–704 in *Proceedings of the 21st Southeastern Conference on Theoretical and Applied Mechanics (SECTAM XXI)*, 2002.

[Xu et al. 2001] S. Xu, X. Deng, A. P. Reynolds, and T. U. Seidel, "Finite element simulation of material flow in friction stir welding", *Sci. Technol. Weld. Joining* **6**:3 (2001), 191–193.

[Zhang and Zhang 2005] Z. Zhang and H. W. Zhang, "The 3D simulation of friction stir welding process", pp. 1338–1342 in *International conference on mechanical engineering and mechanics* (Nanjing, China), 2005.

[Zhang et al. 2005a] H. W. Zhang, Z. Zhang, and J. T. Chen, "Effect of angular velocity of the pin on material flow during friction stir welding", *Acta Metall. Sin.* **41** (2005), 853–869. In Chinese.

[Zhang et al. 2005b] H. W. Zhang, Z. Zhang, and J. T. Chen, "The finite element simulation of the friction stir welding process", *Mater. Sci. Eng. A* **403**:1-2 (2005), 340–348.

[Zhu and Chao 2004] X. K. Zhu and Y. J. Chao, "Numerical simulation of transient temperature and residual stresses in friction stir welding of 304L stainless steel", *J. Mater. Process. Technol.* **146**:2 (2004), 263–272.

Received 8 Aug 2006. Revised 7 Nov 2006. Accepted 27 Feb 2007.

ZHAO ZHANG: zhangz@dlut.edu.cn
Department of Engineering Mechanics, State Key Laboratory of Structural Analysis for Industrial Equipment, Dalian University of Technology, Dalian 116024, China

HONGWU ZHANG: zhanghw@dlut.edu.cn
Department of Engineering Mechanics, State Key Laboratory of Structural Analysis for Industrial Equipment, Dalian University of Technology, Dalian 116024, China